Available online at www.sciencedirect.com

SciVerse ScienceDirect

Ceramics International 38 (2012) 1851–1858

CERAMICS INTERNATIONAL

www.elsevier.com/locate/ceramint

Oxy-apatite reaction sintering of colloidal and classic ceramic processed powders

José M. Porras-Vázquez, Enrique R. Losilla, Miguel A.G. Aranda, Isabel Santacruz *

Departamento de Química Inorgánica, Cristalografía y Mineralogía, Universidad de Málaga, 29071 Málaga, Spain

Received 28 June 2011; received in revised form 26 September 2011; accepted 3 October 2011
Available online 8 October 2011

Abstract

Oxy-apatites are promising electrolyte materials for intermediate-temperature solid oxide fuel cells, IT–SOFC. However the requirements of electrolytes make necessary the preparation of dense films with the appropriated composition to show good electrical properties; in this way, colloidal processing is a key issue.

This work involves the application of colloidal processing for four oxygen-excess oxy-apatites, $La_{9.67}(Si_6O_{24})O_{2.5}$, $La_{10}(Si_6O_{24})O_3$, $La_{10}(Si_{5.5}Al_{0.5}O_{24})O_{2.75}$ and $La_{10}(Si_5Al_1O_{24})O_{2.5}$ and their characterization (phases, microstructure and electrical properties). The results have been compared with those obtained by classical ceramic method to assure the same composition without loosing properties. Samples with the desired compositions were obtained by reaction sintering of La_2O_3, SiO_2 and Al_2O_3. $La_{10}(Si_{5.5}Al_{0.5}O_{24})O_{2.75}$ prepared by colloidal processing and heated at 1923 K showed the highest conductivity value, 3.0×10^{-2} S cm^{-1} at 973 K. Furthermore, its residual porosity was very low. On the other hand, $La_{10}(Si_6O_{24})O_3$ stoichiometry was tried by colloidal and ceramic methods under several experimental conditions. Unfortunately, the obtained oxy-apatite seems to have slightly lower lanthanum content. In spite of previous reports claiming the preparation of stoichiometric $La_{10}(Si_6O_{24})O_3$, this study cannot support these findings.

Keywords: A. Suspensions; A. Powders: solid state reaction; C. Electrical conductivity; D. Apatite; E. Fuel cells

1. Introduction

Solid oxide fuel cells (SOFC) are one of the most promising types of fuel cell for large scale power generation and combined heat and power applications. SOFC offers many advantages over classical combustion-based power generation technologies and has been intensively studied for many years [1–4]. Yttria-stabilized zirconia, YSZ, is the oxide-conducting electrolyte used in the commercial systems. One significant disadvantage with the ZrO_2-based SOFCs is the temperature of operation at which ionic conductivity is sufficiently high for practical applications, usually 1073–1273 K, depending upon the thickness of the electrolyte. To increase the durability of the components, lower operating temperatures are required. Furthermore, to increase performance due to lower overall electrical resistance, thinner (dense) electrolyte films are needed. Hence, developing of new electrolyte materials with higher oxide-conductivities at intermediate temperatures (773–973 K) and the developing of procedures for the preparation and deposition of layers of those electrolytes on porous electrodes is a very important challenge.

Oxy-apatites have high potential to be used as oxide ion conductors working at moderate temperatures, ~973 K [4–8]. They adopt the general formula $A_{10-x}(M_6O_{24})O_{2\pm\delta}$, where A is a rare earth or alkaline earth cation and M is usually a p-block element such as Si, Al, Ge or P. Its structure consists of isolated MO_4 tetrahedra forming channels running parallel to the *c*-axis where the loosely bounded oxide-conducting anions are located. Recent computational studies [9,10] indicated that an unusually broad range of dopant ions (in terms of size and charge state) can substitute for La and Si in the $La_{9.33}(Si_6O_{24})O_2$ parent structure. The observed conductivity is very sensitive to the doping regime and cation–anion non-stoichiometry. The highest conductivities are found for oxygen-excess samples [11], with oxide-ion conduction occurring mainly, but not only, along the oxide-ion channels.

* Corresponding author. Tel.: +34 952 131992; fax: +34 952 131870.
E-mail address: isantacruz@uma.es (I. Santacruz).

0272-8842/$36.00
doi:10.1016/j.ceramint.2011.10.010

One of the main limitation of oxy-apatite materials is related to their poor sinterability [5]. Many researchers have focused their efforts in this key subject by obtaining apatite materials through different routes, such as solid-state reaction [12–15], sol–gel [16–18], hot-pressing techniques [19], initial mechanosyntheses [20,21] facilitating further processing (i.e., colloidal [22]), or precipitate method combined with an azeotropic-distillation process [23]. In addition, electrolytes to be used in SOFCs have to show high densities and low thicknesses. In this way, oxy-apatite tapes and coatings have been recently prepared by tape casting [22,24,25], plasma spraying [26,27] and sputtering [28].

This work is a continuation of our research efforts devoted of the colloidal processing of oxy-apatites with the final goal of obtaining dense thin films of optimum composition(s). Our previous works [29,30] were focused on $La_{10}(Si_5Al_1O_{24})O_{2.5}$. Here, we expand this methodology to improve the processing for $La_{10}(Si_{5.5}Al_{0.5}O_{24})O_{2.75}$, $La_{9.67}(Si_6O_{24})O_{2.5}$ and $La_{10}(Si_6O_{24})O_3$. It is worth noting that we have tried the preparation of the contentious $La_{10}(Si_6O_{24})O_3$. Some groups reported that the preparation of non-doped lanthanum silicon oxy-apatites with very high La-contents by solid state reaction led to the segregation of La_2SiO_5 and the formation of a lanthanum deficient stoichiometry [10,31,32]. On the other hand, other groups assure to be achieved the $La_{10}(Si_6O_{24})O_3$ stoichiometry by classical methods [33,34]. In addition, there are several articles reporting the preparation of this composition by sol–gel [35,36] and precipitation methods [37,38].

2. Experimental

2.1. Synthesis and processing

$La_{9.67}(Si_6O_{24})O_{2.5}$, $La_{10}(Si_6O_{24})O_3$, $La_{10}(Si_{5.5}Al_{0.5}O_{24})O_{2.75}$ and $La_{10}(Si_5Al_1O_{24})O_{2.5}$ were prepared by reaction sintering using high purity oxides: micron powders of La_2O_3 (99.999%, Sigma–Aldrich), γ-Al_2O_3 (99.997%, Alfa Aesar) and SiO_2 (quartz, 99.8%, ABCR). Lanthanum oxide was precalcined at 1000 °C for 2 h for decarbonation. Each composition was prepared by two different synthesis-sintering procedures: the first one, consisting of a colloidal processing of the reagents followed by a reaction sintering step; and a second one, in which was used a single ceramic reaction sintering step. Both of them are described just below.

2.1.1. Colloidal processing

Suspensions with the stoichiometric mixtures of oxides were prepared at a solid loading of 5 wt% (1 vol%) in absolute ethanol by magnetic stirring for 15 min with the addition of the optimum amount of a polymeric dispersant that is soluble in ethanol (Hypermer KD6, Uniqema, Wirrall, UK). The best stabilization was obtained after the addition of 2.0, 2.0 and 3.0 wt% surfactant in dry solid based for La_2O_3, SiO_2 and Al_2O_3 powders, respectively [29]. The apparent pH of these diluted suspensions lies between 8 and 10. The so-prepared suspensions (50 mL) were ultrasonically homogenized using a 400 W sonication probe (UP400s Hielscher Ultrasonics GmbH) for 2 min. Suspensions were cooled in an ice-water bath during ultrasonication in order to avoid excessive heating. Then, the ethanol was evaporated for 24 h in an oven at 338 K. The dried powder was sieved through a 100 μm mesh, and pressed at 640 MPa into 10 mm diameter and 1 mm thickness pellets. After this treatment, samples were heated (heating/cooling rates of 5 K/min) to an intermediate temperature of 1393 K and held for 2 h [30], then the furnace was heated up to the final target temperature, ranged between 1873 and 1923 K (see Table 1) and held at that temperature for 10 h.

Table 1
Temperature of synthesis, theoretical density, secondary phases and electrical conductivity at 973 K for the reported samples.

Composition	Method	T (K)[a]	Density (%) TD	Secondary phases		V/Z (Å^3)	σ_{973} (mS cm^{-1})
				La_2SiO_5 (wt%)	$LaAlO_3$ (wt%)		
$La_{9.67}(Si_6O_{24})O_{2.5}$	Ceramic	1923	85	–	–	588.43(1)	9.5
	Colloidal	1873	68	–	–	588.83(8)	–
		1898	81	–	–	589.26(4)	0.7
		1923	80	–	–	589.17(3)	0.4
$La_{10}(Si_6O_{24})O_3$	Ceramic	1923	80	20.0(1)	–	588.72(1)	–
	Colloidal	1873	84	–	–	588.84(2)	6
		1898	80	7.0(8)	–	588.46(3)	9
		1923	80	Amorphous	–	589.44(4)	
$La_{10}(Si_{5.5}Al_{0.5}O_{24})O_{2.75}$	Ceramic	1873	90	–	–	590.91(1)	24
	Colloidal	1873	80	9.9(2)	1.7(2)	588.96(5)	6
		1898	85	–	–	590.61(4)	25
		1923	88	–	–	591.63(6)	30
$La_{10}(Si_5Al_1O_{24})O_{2.5}$	Ceramic	1873	89	–	–	592.71(1)	21
	Colloidal	1873	84	–	–	Two apatites	17
		1898	84	–	1.6(1)	592.16(5)	17
		1923	94	–	2.0(1)	592.51(6)	12

[a] The dwelling time was always 10 h.

2.1.2. Classical ceramic method

Reagents were ground for 30 min, pelletized (640 MPa, 10 mm diameter and 1 mm thickness) in an agate mortar and heated at a temperature depending on composition, ranged 1873–1923 K (see Table 1) for 10 h at a heating/cooling rate of 5 K/min.

2.2. Powder diffraction

All compounds were characterized by high-resolution laboratory X-ray powder diffraction (LXRPD) at room temperature. Powder patterns were collected using a X'Pert Pro MPD (PANalytical) automated diffractometer equipped with a Ge(1 1 1) primary monochromator (strictly monochromatic CuKα_1 radiation) and an X'Celerator detector. The studied 2θ range was 15–90° with a 0.017° step size. Rietveld analyses [39] were carried out using the GSAS [40] suite of programs.

2.3. Microstructural characterization

The microstructure (morphology and grain size) of the oxy-apatites in the sintered pellets was studied using a JEOL SM 840 scanning electron microscope. The ceramic surfaces were polished with diamond sprays (6, 3, and 1 μm) and thermally etched at 50 K below the sintering temperature for 15 min at a heating/cooling rate of 5 K/min. Finally, the samples were gold sputtered for a better image definition. The grain sizes of sintered pellets were estimated from SEM micrographs using the linear intercept method from at least 30 random lines and three different micrographs with the help of image-analysis software. On the other hand, pellet compactions were calculated taking into account the pellet mass, volume (from the face area and thickness, assuming a perfect cylinder) and the crystallographic density.

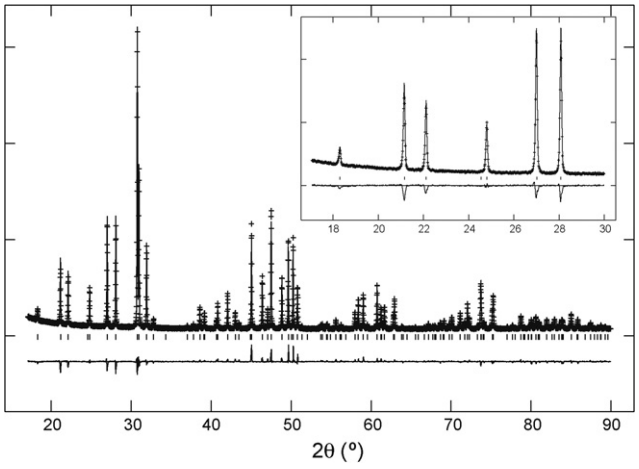

Fig. 1. Observed (crosses), calculated (full line), and difference curve (bottom) X-ray laboratory powder diffraction patterns for '$La_{10}(Si_6O_{24})O_3$' prepared by colloidal processing at 1873 K for 10 h. The inset shows the low angle region to highlight the absence of crystalline impurity phases.

2.4. Electrical characterization

Electrodes were prepared by coating opposite pellet faces with a METALOR® 6082 platinum paste and gradually heating to 1223 K at a rate of 10 K/min in air to decompose the paste and harden the Pt residue. Successive treatments were carried out to achieve an electrical resistance of both pellet faces lower than 1 Ω. Impedance spectroscopy data were collected in air using an HP4284A (Agilent Technologies) impedance analyzer over the frequency range from 20 Hz to 1 MHz with an applied voltage of 0.1 V. Electrical measurements were taken on cooling in the temperature range of 573–1273 K every 25 K (accuracy of 1 K) at 10 K/min with a delay time of 30 min at each temperature to ensure thermal stabilization. Measurements were controlled by the winDETA package of programs (Novocontrol GmbH).

3. Results and discussion

3.1. Synthesis and samples stoichiometries

The synthesis-sintering conditions and some key physical properties for the compositions prepared by both procedures are shown in Table 1. All pellets were ground and their powder patterns were analyzed by the Rietveld method using the structural description previously reported for $La_{9.5}\square_{0.5}(Si_{5.5}Al_{0.5}O_{24})O_2$ [41] as starting model. The occupation factors for lanthanum, silicon, and aluminium sites were conveniently modified to describe their stoichiometries. Only the overall parameters (histogram scale factor, background coefficients, unit cell parameters, zero-shift error, and peak shape pseudo-Voigt coefficients) and weight fractions of side phases (if necessary) were refined. Atomic parameters were not optimized. Final Rietveld refinements showed good figures of merit with R_F ranging between 3% and 6%. As an example of refinement quality, the Rietveld plot for '$La_{10}(Si_6O_{24})O_3$', prepared by colloidal processing at 1873 K for 10 h, is shown in Fig. 1.

3.1.1. Aluminium-free lanthanum oxy-apatites

For preparing $La_{9.67}(Si_6O_{24})O_{2.5}$ and $La_{10}(Si_6O_{24})O_3$ stoichiometries, the thermal cycle applied in dry ceramic conditions was a single heating/cooling cycle up to 1923 K for 10 h (see Table 1). For the colloidal processing, the cycle was a step to 1393 K for 2 h, followed of a final target temperature, ranged 1873–1923 K [29]. $La_{9.67}(Si_6O_{24})O_{2.5}$ was obtained as single-phase by both procedures at all temperatures. However, below 1898 K the density values achieved were very low (see Table 1). Furthermore, the unit cell volume values obtained from Rietveld analysis for $La_{9.67}(Si_6O_{24})O_{2.5}$ samples (see Table 1) display important differences between the synthesis procedures, almost 0.8 Å^3. This behaviour may be due to the fact that samples prepared from colloidal processing need higher sintering temperatures than those obtained by classical ceramic method to achieve the same compaction. This is tentatively assigned to a possible carbonation of La_2O_3 powder when the suspension was dried; hence that carbonated

powder would produce samples with lower green density values which would need higher sintering temperature.

On the other hand, '$La_{10}(Si_6O_{24})O_3$' samples obtained by colloidal processing showed only a single crystalline phase after sintering the green sample at 1873 K for 10 h (see Table 1 and Fig. 1). Higher sintering temperatures lead to segregation of large amounts of La_2SiO_5 or partial decomposition of the colloidal-sample. This behaviour strongly suggests that this composition is not thermodynamically stable. This observation is in agreement with some reports where this stoichiometry could not be achieved by a classical solid state reaction [33,34] and it seems to be necessary a mild pre-preparation (sol–gel, co-precipitation, etc.) before the high temperature synthesis–sintering cycles [35–38]. For '$La_{10}(Si_6O_{24})O_3$' obtained by colloidal processing at 1873 K, the Rietveld analysis gave a unit cell volume of 588.84(2) Å^3. The similar analysis for $La_{9.67}(Si_6O_{24})O_{2.5}$ prepared under the same conditions gave 588.83(2) Å^3 (see Table 1). Therefore, there is not unit cell variation between both stoichiometries. Furthermore, a small unit cell expansion is expected with the La content in the $La_{9.33+x}(Si_6O_{24})O_{2+3x/2}$ series as previously reported [42]. Hence, although '$La_{10}(Si_6O_{24})O_3$' is a single crystalline phase, the sample stoichiometry (and hence its critical high oxygen content) need to be ensured. Therefore, we have carried out two Rietveld analysis by refining La(1) occupation factor while keep fixed the La(2) occupation factor, and the other way around. This procedure is needed to avoid the correlation between the La occupation factor(s) and the overall histogram scale factor. It is worth keeping in mind that La(1) it is always fully occupied and the La vacancies (if present) are located at the La(2) site [7]. The Rietveld refinement keeping the occupation factor of La(2) fixed converged to $R_F = 6.0\%$ and La(1) occupation factor = 1.041(5). Conversely, the second analysis gave $R_F = 5.1\%$ and La(2) occupation factor = 0.891(5). Therefore, the similarity between the unit cell volumes and the observed deficiency at the La(2) position points towards the crystalline oxy-apatite phase being La-deficient. So, our study does not support the '$La_{10}(Si_6O_{24})O_3$' stoichiometry and neutron powder diffraction will be used to fully settle this point.

Aluminium-doped lanthanum oxy-apatites. For Al-doped lanthanum silicon apatites, the optimum sintering conditions were a single heating/cooling cycle at 1873 K for 10 h for the classical ceramic preparations. Lower temperatures led to poorer relative densities. By colloidal processing, the thermal cycle used was a step at 1393 K for 2 h, followed of a final target temperature ranged 1873–1923 K [29]. Temperatures below 1898 K led to the segregation of secondary phases for $La_{10}(Si_{5.5}Al_{0.5}O_{24})O_{2.75}$, and the formation of two types of (very related) apatites for $La_{10}(Si_5Al_1O_{24})O_{2.5}$ (Table 1). For $La_{10}(Si_{5.5}Al_{0.5}O_{24})O_{2.75}$ composition, temperatures higher than 1923 K drifted to the partial melting of these compositions. For $La_{10}(Si_5Al_1O_{24})O_{2.5}$, even at 1923 K there was an indication of partial melting. Furthermore, for this sample it was observed segregation of a minor amount of $LaAlO_3$. Volume values for Al-doped compositions are larger than those of non-doped compositions. Unit cell volumes for $La_{10}(Si_5Al_1O_{24})O_{2.5}$ are bigger than for $La_{10}(Si_{5.5}Al_{0.5}O_{24})O_{2.75}$, as expected since the ionic radii of Al^{3+} (0.39 Å) is larger than that of Si^{4+} (0.26 Å). Overall, the unit cell variations support the formation of the nominal stoichiometries.

3.2. Microstructures

Pellets densities are reported in Table 1. It must be highlighted that high compactions are needed for electrolytes in order to avoid gas diffusion between the electrodes. It can be seen in Table 1 that for the same stoichiometry and final

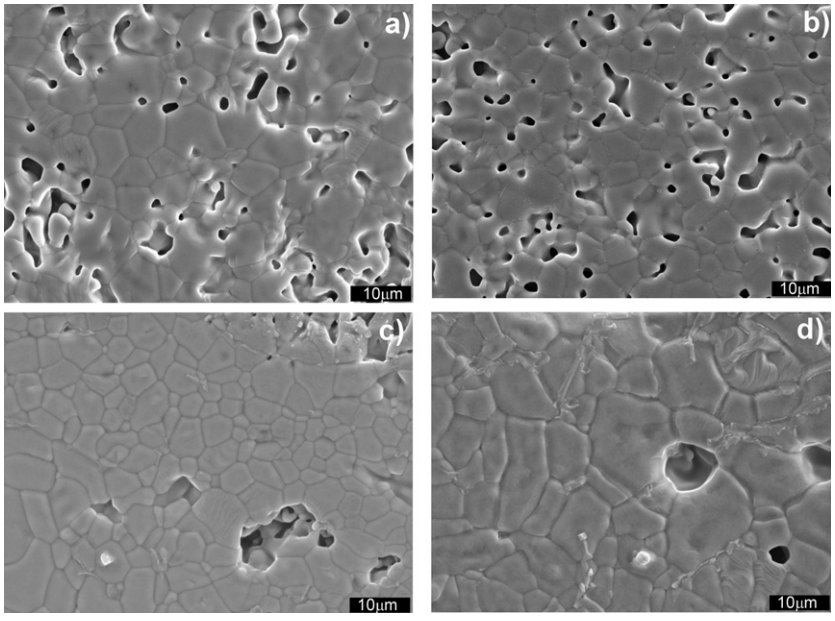

Fig. 2. SEM micrographs for the samples prepared by colloidal processing at selected conditions. (a) $La_{9.67}(Si_6O_{24})O_{2.5}$ at 1898 K for 10 h; (b) $La_{10}(Si_6O_{24})O_3$ at 1873 K for 10 h; (c) $La_{10}(Si_{5.5}Al_{0.5}O_{24})O_{2.75}$ at 1923 K for 10 h; and (d) $La_{10}(Si_5Al_1O_{24})O_{2.5}$ at 1898 K for 10 h.

sintering temperature, the obtained densities are always slightly larger for the ceramic method that for the colloidal process. This may be justified by a partial carbonation of the lanthanum oxide reagent during processing. Alternatively, it may be also due to the low solid contents of the initial suspensions. More work is underway in this direction.

SEM micrographs for the four compositions prepared by colloidal processing, with the better electrical properties (see below) are shown in Fig. 2. The micrographs were analyzed to evaluate both the grain size distribution and the estimated average grain size. The grain size distributions showed a Gaussian-like pattern and the extracted average grain sizes. The average grain sizes for colloidal processing oxy-apatites sintered at 1898 K for 10 h were 5.8, 5.5 and 6.6 μm for $La_{9.67}(Si_6O_{24})O_{2.5}$, $La_{10}(Si_{5.5}Al_{0.5}O_{24})O_{2.75}$ and $La_{10}(Si_5Al_1O_{24})O_{2.5}$, respectively. Colloidal $La_{10}(Si_6O_{24})O_3$ was sintered at 1873 K showing 4.7 μm of average grain size. Both aluminium-doped apatite samples prepared by the conventional ceramic method and sintered at 1873 K showed an average grain size of ~3 μm, lower than the equivalent compositions prepared by colloidal processing (and sintered at 1898 K). The difference in grain size can be attributed to the lower sintering temperature used in the ceramic method.

Finally, it is worth pointing out that the densities obtained from the pellet mass and volumes seem to be smaller than the values deduced from the SEM images for Al-containing oxy-apatites, see Table 1 and Fig. 2. This discrepancy is likely due to a small curvature observed for these pellets after sintering at high temperature. This (small) curvature makes the calculation of the pellet volumes only approximate.

3.3. Electrical characterization

Impedance spectroscopy was used to determine the electrical conductivity data for pellets with a relative density larger than 80% of the theoretical density. Representative impedance data are reported in Fig. 3. Similar Nyquist plots were obtained for the remaining compositions. At low temperatures (not shown), a set of overlapping semicircles was observed, likely due to the grain interior (bulk) and to internal interfaces (grain boundary and/or porosity). Lower frequency processes were observed in the form of a spike. At 973 K (see Fig. 3) the spike collapses to a semicircular arc, indicating that oxygen molecules are able to diffuse through the entire thickness of the electrode. In order to quantitatively estimate bulk and grain-boundary conductivities of the samples, complex impedance spectra were analyzed by nonlinear least squares fittings of equivalent circuits using the program Zview [43]. Associated errors were high, and hence, the values are not reported here. Selected overall conductivities were plotted in a traditional Arrhenius format (see Fig. 4), and they fall on a set of straight lines.

3.3.1. Aluminium-free lanthanum oxo-apatites

$La_{9.67}(Si_6O_{24})O_{2.5}$ samples prepared by classical ceramic method and sintered at 1923 K (see Table 1) showed a

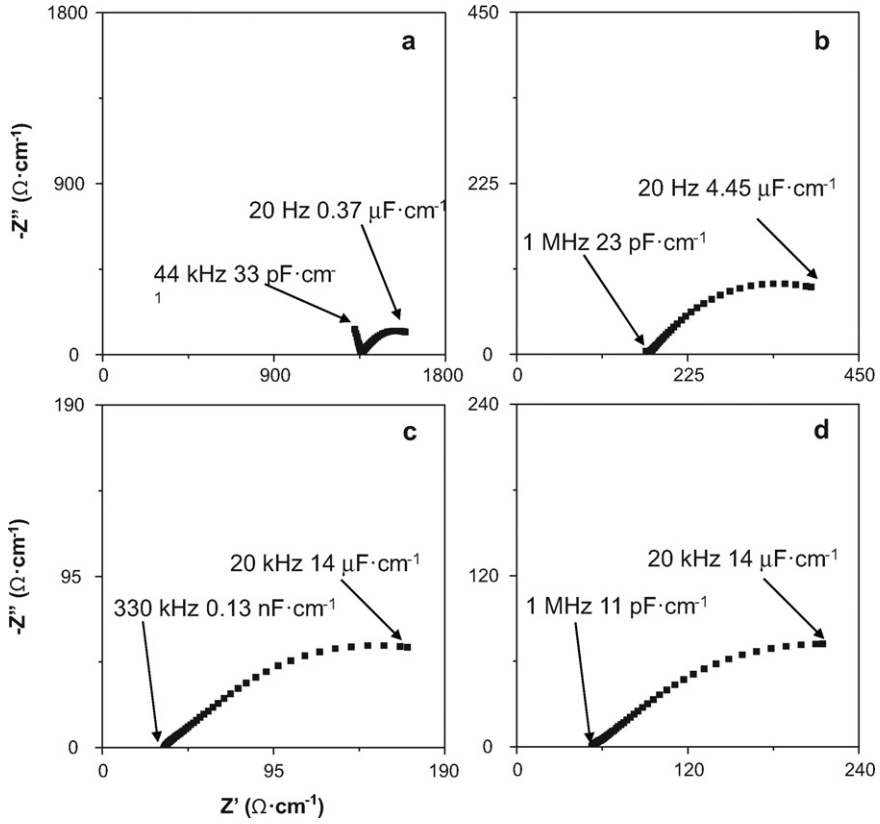

Fig. 3. Complex impedance plane plots at 973 K for the samples prepared by colloidal processing. (a) $La_{9.67}(Si_6O_{24})O_{2.5}$, 1898 K 10 h; (b) $La_{10}(Si_6O_{24})O_3$, 1873 K 10 h; (c) $La_{10}(Si_{5.5}Al_{0.5}O_{24})O_{2.75}$, 1923 K 10 h; and (d) $La_{10}(Si_5Al_1O_{24})O_{2.5}$, 1898 K 10 h.

conductivity value at 973 K of 1.1×10^{-2} S cm^{-1}. The same stoichiometry prepared by colloidal processing and sintered at 1898 K gave 0.7×10^{-3} S cm^{-1}. There is one order of magnitude of difference. This behaviour is likely due to possible inhomogeneities in the samples during the processing and their relatively low pellet densities.

For colloidally processed '$La_{10}(Si_6O_{24})O_3$', sintered at 1873 K, the overall conductivity at 973 K was 0.6×10^{-2} S cm^{-1}. This value is lower than that reported by Nojiri et al. [33], 2.1×10^{-2} S cm^{-1} at 973 K, for a sample prepared by classical ceramic method with a final sintering temperature of 1953 K. However, the value reported in this work is close to that given by Li et al. [38], 1.2×10^{-2} S cm^{-1} at 973 K, for a sample prepared by co-precipitation and a final step at 1923 K. The spread in conductivity values for this stoichiometry may be due to the residual porosities but also to the different real lanthanum stoichiometries of the oxy-apatite framework.

3.3.2. Aluminium-doped lanthanum oxo-apatites

$La_{10}(Si_{5.5}Al_{0.5}O_{24})O_{2.75}$ prepared by ceramic method and sintered at 1873 K gave an overall conductivity of 2.4×10^{-2} S cm^{-1} at 973 K. The same stoichiometry colloidally processed and sintered at 1923 K gave an overall conductivity of 3.0×10^{-2} S cm^{-1} at 973 K. These conductivity values are quite close and in very good agreement with that previously reported by Shaula et al. [44] for the same composition, $\sim 3.0 \times 10^{-2}$ S cm^{-1} at 973 K. These very high conductivity values, the absence of secondary phases and the reproducibility of the measurements for different processing strategies make this composition a very attractive candidate as SOFC electrolyte when to be colloidally processed as dense thin films.

$La_{10}(Si_5Al_1O_{24})O_{2.5}$ prepared by ceramic method and sintered at 1873 K gave an overall conductivity of 2.1×10^{-2} S cm^{-1} at 973 K. The same stoichiometry colloidally processed and sintered at 1898 K gave an overall conductivity of 1.7×10^{-2} S cm^{-1} at 973 K. Higher temperatures led to lower conductivity values, likely due to partial melting of the sample. This conductivity values are quite close to that previously reported for the same stoichiometry, 2.9×10^{-2} S cm^{-1} at 973 K [44].

Finally, two regimes with different activation energies are observed in the Arrhenius plot, as found for related oxygen-excess oxy-apatite materials [45,46]. Below 1023 K, the activation energy ranges between 0.98(3) and 0.69(1) eV. Above 1023 K, the activation energies are much smaller, ranging between 0.35(1) and 0.58(1) eV. This curvature is usually explained by the presence of a critical temperature, T_c, [47] below which the charge carriers are progressively trapped, which increases the overall activation energies.

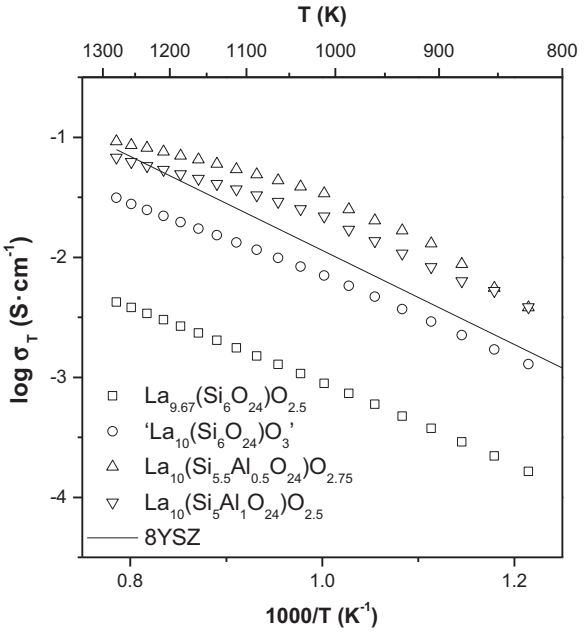

Fig. 4. Arrhenius plot of $\log \sigma_T$ of colloidal processed oxy-apatites. $La_{9.67}(Si_6O_{24})O_{2.5}$, $La_{10}(Si_{5.5}Al_{0.5}O_{24})O_{2.75}$ and $La_{10}(Si_5Al_1O_{24})O_{2.5}$ were sintered at 1898 K. $La_{10}(Si_6O_{24})O_3$ was sintered at 1873 K. The conductivity values for 8YSZ (line) are also shown for the sake of comparison.

4. Conclusions

$La_{9.67}(Si_6O_{24})O_{2.5}$, '$La_{10}(Si_6O_{24})O_3$', $La_{10}(Si_{5.5}Al_{0.5}O_{24})O_{2.75}$ and $La_{10}(Si_5Al_1O_{24})O_{2.5}$ oxy-apatites were prepared by colloidal processing and characterized. All the final pellets were obtained by reaction sintering. The properties have been compared with those obtained by classical ceramic method. Colloidal processed samples required higher sintering temperatures for achieving the same final density values than those obtained by the classical ceramic method. Samples with densities up to 94% of the theoretical densities were obtained showing high oxide conductivities values. Electron microscopy characterization indicated that the aluminium-containing samples have very low residual porosities for both preparation methods. The electrical properties of the samples prepared by colloidal processing are very similar to those obtained by classical methods, so we can affirm that the studied compositions can successfully be prepared by colloidal process despite some carbonation during drying. Moreover, it is highlighted that colloidally processed $La_{10}(Si_{5.5}Al_{0.5}O_{24})O_{2.75}$ showed a conductivity value of 3.0×10^{-2} S cm^{-1} at 973 K, with very low porosity and without secondary phases. These properties make this sample very attractive as IT–SOFCs electrolyte. These results are promising for the conformation of the electrolytes as films and confirm the colloidal processing as a very useful procedure for developing oxy-apatites with good electrical properties. Finally, the contentious '$La_{10}(Si_6O_{24})O_3$' stoichiometry was tried by the two procedures; however, the results point towards the stabilization of a lanthanum deficient oxy-apatite with a stoichiometry close to $La_{9.7}(Si_6O_{24})O_{2.55}$.

Acknowledgements

This work has been supported by Junta de Andalucía (Spain) through the P10-FQM-6680 research grant. Financial help from

AP2005-2462 studentship, and Ramón y Cajal fellowship (RYC-2008-03523) is also acknowledged.

References

[1] R.M. Ormerod, Solid oxide fuel cells, Chem. Soc. Rev. 32 (2003) 17–28.

[2] N.P. Brandon, S. Skinner, B.C.H. Steele, Recent advances in materials for fuel cells, Annu. Rev. Mater. Res. 33 (2003) 183–213.

[3] J.W. Fergus, Electrolytes for solid oxide fuel cells, J. Power Sources 162 (2006) 30–40.

[4] J.W. Fergus, R. Hui, X. Li, D.P. Wilkinson, J. Zhang, Solid oxide fuel cells, in: Materials Properties and Performance, CRC Press, Taylor & Francis Group, Boca Ratón, FL, 2009.

[5] P.J. Panteix, I. Julien, P. Abélard, D. Bernache-Assollant, Influence of porosity on the electrical properties of $La_{9.33}(SiO_4)_6O_2$ oxyapatite, Ceram. Int. 34 (2008) 1579–1586.

[6] E.J. Abram, D.C. Sinclair, A.R. West, A novel enhancement of ionic conductivity in the cation-deficient apatite $La_{9.33}(SiO_4)_6O_2$, J. Mater. Chem. 11 (2001) 1978–1979.

[7] L. León-Reina, E.R. Losilla, M. Martinez-Lara, S. Bruque, M.A.G. Aranda, Interstitial oxygen conduction in lanthanum oxy-apatite electrolytes, J. Mater. Chem. 14 (2004) 1142–1149.

[8] D. Marrero-López, M.C. Martín-Sedeño, J. Peña-Martínez, J.C. Ruiz-Morales, P. Núñez, M.A.G. Aranda, J.R. Ramos-Barrado, Evaluation of apatite silicates as solid oxide fuel cell electrolytes, J. Power Sources 195 (2010) 2496–2506.

[9] J.R. Tolchard, P.R. Slater, M.S. Islam, Insight into doping effects in apatite silicate ionic conductors, Adv. Funct. Mater. 17 (2007) 2564–2571.

[10] E. Kendrick, M.S. Islam, P.R. Slater, Developing apatites for solid oxide fuel cells: insight into structural, transport and doping properties, J. Mater. Chem. 17 (2007) 3104–3111.

[11] H. Yoshioka, Y. Nojiri, S. Tanase, Ionic conductivity and fuel cell properties of apatite-type lanthanum silicates doped with Mg and containing excess oxide ions, Solid State Ionics 179 (2008) 2165–2169.

[12] Y. Ohnishi, A. Mineshige, Y. Daiko, M. Kobune, H. Yoshioka, T. Yazawa, Effect of transition metal additives on electrical conductivity for La-excess-type lanthanum silicate, Solid State Ionics 181 (2010) 1697–1701.

[13] A. Vincent, S.B. Savignat, F. Gervais, Elaboration and ionic conduction of apatite-type lanthanum silicates doped with Ba, $La_{10-x}Ba_x(SiO_4)_6O_{3-x/2}$ with $x = 0.25–2$, J. Eur. Ceram. Soc. 27 (2007) 1187–1192.

[14] Y. Higuchi, M. Sugawara, K. Onishi, M. Sakamoto, S. Nakayama, Oxide ionic conductivities of apatite-type lanthanum silicates and germanates and their possibilities as an electrolyte of lower temperature operating SOFC, Ceram. Int. 36 (2010) 955–959.

[15] A. Mineshige, T. Nakao, Y. Ohnishi, R. Sakamoto, Y. Daiko, M. Kobune, T. Yazawa, H. Yoshioka, T. Fukutsuka, Y. Uchimoto, Ionic and electronic conductivities and fuel cell performance of oxygen excess-type lanthanum silicates, J. Electrochem. Soc. 157 (2010) B1465–B1470.

[16] E. Jothinathan, K. Vanmeensel, J. Vleugels, O. Van der Biest, Powder synthesis, processing and characterization of lanthanum silicates for SOFC application, J. Alloys Compd. 495 (2010) 552–555.

[17] S.W. Tao, J.T.S. Irvine, Preparation and characterization of apatite-type lanthanum silicates by a sol–gel process, Mater. Res. Bull. 36 (2001) 1245–1258.

[18] Y. Wenhui, S. Rongping, L. Li, Chin. Synthesis and Conductivity of Oxyapatite Ionic Conductor $La_{10-x}V_x(SiO_4)_6O_{3+x}$, J. Chem. Eng. 18 (2010) 328–332.

[19] P.J. Panteix, I. Julien, D. Bernache-Assollant, P. Abelard, Synthesis and characterization of oxide ions conductors with the apatite structure for intermediate temperature SOFC, Mater. Chem. Phys. 95 (2005) 313–320.

[20] L.G. Martínez-González, E. Rodríguez-Reyna, K.J. Moreno, J.I. Escalante-García, A.F. Fuentes, Ionic conductivity of apatite-type rare-earth silicates prepared by mechanical milling, J. Alloys Compd. 476 (2009) 710–714.

[21] A.F. Fuentes, E. Rodríguez-Reyna, L.G. Martínez-González, M. Maczka, J. Hanuza, U. Amador, Room-temperature synthesis of apatite-type lanthanum silicates by mechanically milling constituent oxides, Solid State Ionics 177 (2006) 1869–1873.

[22] C. Bonhomme, S. Beaudet-Savignat, T. Chartier, P.M. Geffroy, A.L. Sauvet, Evaluation of the $La_{0.75}Sr_{0.25}Mn_{0.8}Co_{0.2}O_{3-\delta}$ system as cathode material for ITSOFCs with $La_9Sr_1Si_6O_{26.5}$ apatite as electrolyte, J. Eur. Ceram. Soc. 29 (2009) 1781–1788.

[23] H.C. Yao, J.S. Wang, D.G. Hu, J.F. Li, X.R. Lu, Z.J. Li, New approach to develop dense lanthanum silicate oxy-apatite sintered ceramics with high conductivity, Solid State Ionics 181 (2010) 41–47.

[24] C. Bonhomme, S. Beaudet-Savignat, T. Chartier, C. Pirovano, R.N. Vannier, Elaboration, by tape casting, and thermal characterization of a solid oxide fuel half-cell for low temperature applications, Mater. Res. Bull. 45 (2010) 491–498.

[25] C. Bonhomme, S. Beaudet-Savignat, T. Chartier, A. Maître, A.L. Sauvet, B. Soulestin, Sintering kinetics and oxide ion conduction in Sr-doped apatite-type lanthanum silicates, $La_9Sr_1Si_6O_{26.5}$, Solid State Ionics 180 (2009) 1593–1598.

[26] S. Dru, E. Meillot, K. Wittmann-Teneze, R. Benoit, M.L. Saboungi, Plasma spraying of lanthanum silicate electrolytes for intermediate temperature solid oxide fuel cells (ITSOFCs), Surf. Coat. Tech. 205 (2010) 1060–1064.

[27] H. Yoshioka, T. Mitsui, A. Mineshige, T. Yazawa, Fabrication of anode supported SOFC using plasma-sprayed films of the apatite-type lanthanum silicate as an electrolyte, Solid State Ionics 181 (2010) 1707–1712.

[28] C.Y. Ma, P. Briois, J. Böhlmark, F. Lapostoll, A. Billard, $La_{9.33}Si_6O_{26}$ electrolyte thin films for IT–SOFC application deposited by a HIPIMS/DC hybrid magnetron sputtering process, Ionics 14 (2008) 471–476.

[29] I. Santacruz, J.M. Porras-Vázquez, E.R. Losilla, M.A.G. Aranda, Preparation of aluminium lanthanum oxyapatite tapes, $La_{10}AlSi_5O_{26.5}$, by tape casting and reaction sintering, J. Eur. Ceram. Soc. 31 (2011) 1573–1580.

[30] I. Santacruz, J.M. Porras-Vázquez, E.R. Losilla, M.I. Nieto, R. Moreno, M.A.G. Aranda, Colloidal processing and characterization of aluminum-doped lanthanum oxyapatite, $La_{10}AlSi_5O_{26.5}$, J. Am. Ceram. Soc. 94 (2011) 224–230.

[31] L. León-Reina, E.R. Losilla, M. Martínez-Lara, S. Bruque, M.A.G. Aranda, Interstitial oxygen conduction in lanthanum oxy-apatite electrolytes, J. Mater. Chem. 14 (2004) 1142–1149.

[32] P.R. Slater, J.E.H. Sansom, J.R. Tolchard, Development of apatite-type oxide ion conductors, Chem. Rec. 4 (2004) 373.

[33] Y. Nojiri, S. Tanase, M. Iwasa, H. Yoshioka, Y. Matsumura, T. Sakai, Ionic conductivity of apatite-type solid electrolyte material, $La_{10-X}Ba_XSi_6O_{27-X/2}$ ($X = 0–1$), and its fuel cell performance, J. Power Sources 195 (2010) 4059–4064.

[34] A. Mineshige, T. Nakao, M. Kobune, T. Yazawa, H. Yoshioka, Electrical properties of $La_{10}Si_6O_{27}$-based oxides, Solid State Ionics 179 (2008) 1009–1012.

[35] N. Nallamuthu, I. Prakash, N. Satyanarayana, M. Venkateswarlu, Electrical conductivity studies of nanocrystalline lanthanum silicate synthesized by sol–gel route, J. Alloys Compd. 509 (2011) 1138–1145.

[36] S.P. Jiang, L. Zhang, H.Q. He, R.K. Yap, Y. Xiang, Synthesis and characterization of lanthanum silicate apatite by gel-casting route as electrolytes for solid oxide fuel cells, J. Power Sources 189 (2009) 972–981.

[37] S.H. Jo, P. Muralidharan, D.K. Kim, Raman and ^{29}Si NMR spectroscopic characterization of lanthanum silicate electrolytes: emphasis on sintering temperature to enhance the oxide-ion conductivity, Electrochim. Acta 54 (2009) 7495–7501.

[38] B. Li, W. Liu, W. Pan, Synthesis and electrical properties of apatite-type $La_{10}Si_6O_{27}$, J. Power Sources 195 (2010) 2196–2201.

[39] H.M. Rietveld, A profile refinement method for nuclear and magnetic structures, J. Appl. Cryst. 2 (1969) 65–71.

[40] A. C. Larson, R. B. V. Dreele, General Structure Analysis System (GSAS) program. Rep. No. LA-UR-86748, Los Alamos National Laboratory, Los Alamos, CA, 1994.

[41] L. León-Reina, J.M. Porras-Vázquez, E.R. Losilla, M.A.G. Aranda, Interstitial oxide positions in oxygen-excess oxy-apatites, Solid State Ionics 177 (2006) 1307–1315.

[42] A. Chesnaud, G. Dezanneau, C. Estournès, C. Bogicevic, F. Karolak, S. Geiger, G. Geneste, Influence of synthesis route and composition on

electrical properties of $La_{9.33+x}Si_6O_{26+3x/2}$ oxy-apatite compounds, Solid State Ionics 179 (2008) 1929–1939.

[43] D. Johnson, ZView, A Software Program for IES Analysis, Version 2.9a, Scribner Associates Inc., Southern Pines, NC, 1990–2005.

[44] A.L. Shaula, V.V. Kharton, F.M.B. Marques, Oxygen ionic and electronic transport in apatite-type $La_{10-x}(Si,Al)_6O_{26\pm\delta}$, J. Solid State Chem. 178 (2005) 2050–2061.

[45] L. León-Reina, M.C. Martín-Sedeño, E.R. Losilla, A. Cabeza, M. Martínez-Lara, S. Bruque, F.M.B. Marques, D.V. Sheptyakov, M.A.G. Aranda, Crystalchemistry and oxide ion conductivity in the lanthanum oxygermanate apatite series, Chem. Mater. 15 (2003) 2099–2108.

[46] L. León-Reina, E.R. Losilla, M. Martínez-Lara, M.C. Martín-Sedeño, S. Bruque, P. Núñez, D.V. Sheptyakov, M.A.G. Aranda, High oxide ion conductivity in al-doped germanium oxyapatite, Chem. Mater. 17 (2005) 596–600.

[47] K. Huang, R.S. Tichy, J.B. Goodenough, Superior perovskite oxide-ion conductor; strontium- and magnesium-doped $LaGaO_3$: I, phase relationships and electrical properties, J. Am. Ceram. Soc. 81 (1998) 2565–2575.